Applied Physics Letters

RESEARCH ARTICLE | JULY 13 2015

Junction optimization in HgCdTe: Shockley-Read-Hall generation-recombination suppression FREE

J. Schuster; R. E. DeWames; E. A. DeCuir, Jr.; E. Bellotti; P. S. Wijewarnasuriya

Appl. Phys. Lett. 107, 023502 (2015)
https://doi.org/10.1063/1.4926603

AIP Publishing

Junction optimization in HgCdTe: Shockley-Read-Hall generation-recombination suppression

J. Schuster,[1,2,a)] R. E. DeWames,[3] E. A. DeCuir, Jr.,[1] E. Bellotti,[2] and P. S. Wijewarnasuriya[1]
[1]U.S. Army Research Laboratory, 2800 Powder Mill Road, Adelphi, Maryland 20783, USA
[2]Department of Electrical and Computer Engineering, Boston University, 8 St. Marys Street, Boston, Massachusetts 02215, USA
[3]Fulcrum Company, 5870 Trinity Parkway, Suite 400. Centreville, Virginia 20120, USA

(Received 10 April 2015; accepted 30 June 2015; published online 13 July 2015)

Heterojunction device design concepts are leveraged to reduce depletion layer generation-recombination (G-R) dark current in planar P^+-on-n SWIR HgCdTe infrared detectors. Shockley-Read-Hall (SRH) depletion dark current (when present) is expected to be the dominant dark current component at low temperatures, and in fact, it is beneficial for the transition from diffusion to G-R to be at such relatively low temperatures. However, it is empirically observed that even for relatively long values of the SRH lifetime (20 μs), the transition occurs at relatively high temperatures (>200 K) for material with a cut-off wavelength of 2.5 μm. A key device design parameter of P^+-on-n photodiodes is the position of the electrical junction relative to the hetero-metallurgical interface. Junction formation via p-type arsenic implantation into the narrow-gap absorber layer is typically chosen for efficient collection of diffusion current, however, other configurations are possible as well. In this letter, we numerically explore the conditions that reduce depletion dark current without reducing the quantum efficiency (QE). The findings support the assertion that device design conditions exist in SWIR HgCdTe that essentially eliminate the depletion dark current without significantly reducing the QE. © *2015 AIP Publishing LLC*. [http://dx.doi.org/10.1063/1.4926603]

Recently, the U.S. Army and the other services have become increasingly interested in pursuing imaging capabilities in the short-wave infrared (SWIR) spectral window ($1-3\,\mu$m). The $1.3-1.7\,\mu$m spectral band has garnered the most attention over the years, but recent efforts are now focusing in the extended-SWIR (eSWIR, $1.7-3.0\,\mu$m) band.[1] However, passive imaging in these bands under full moon or starlight conditions requires systems with extremely low noise, due to the relatively low photon fluxes available in these bands.[2] In this regard, one source of noise that may limit the overall system performance arises from dark current in the device material that comes from fundamental or defect-related mechanisms. While achieving dark current contributions from only fundamental mechanisms should be the goal for best case device performance, it may not be readily achievable with current technology and/or resources.

$In_{0.53}Ga_{0.47}As$, lattice matched to InP, is widely used for imaging in the spectral band from $0.8-1.7\,\mu$m. It is well known that extending InGaAs beyond 1.7 μm creates lattice-mismatched growth conditions on InP substrates. This typically results in additional defect related dark current over its lattice-matched counterpart.[1] However, perhaps a more important limitation is a severe reduction in quantum efficiency (QE) due to the relatively large band offsets[3] present in heterojunction[4] architectures which may be employed to reduce Shockley-Read-Hall (SRH) junction dark current. In contrast, the $Hg_{1-x}Cd_xTe$ material system is nearly lattice matched[5] for alloy compositions with cut-off wavelengths ranging from $\lambda_c = 1.8-16.0\,\mu$m. Band offsets in HgCdTe are relatively small,[6] which enables depletion dark current reduction designs with no significant reduction in QE.

Diffusion limited SWIR ($\lambda_c = 2.5\,\mu$m) HgCdTe devices (Auger and radiative recombination) are capable of achieving a dark current as low as $\sim 1\,nA/cm^2$ at 200 K, essential to imaging in the SWIR and eSWIR due to the very low photon fluxes. However, non-optimized growth conditions may present material defects in HgCdTe leading to SRH recombination dominated dark current. In fact, a modest SRH lifetime of 20 μs (Ref. 7) increases the dark current significantly in SWIR HgCdTe. The natural solution to reduce SRH recombination, to regain diffusion limited performance, is by reducing the number of defects during growth/device processing, which may not be immediately obvious or possible. It is, therefore, desirable to explore design principles that minimize the SRH dark current contribution without requiring significant defect reduction. In this letter, numerical simulations are leveraged to incorporate intelligent heterojunction[4] device design which engineers effective suppression of SRH G-R dark current, thereby recovering diffusion limited behavior.

The analysis begins by considering a single large-area eSWIR planar P^+-on-n HgCdTe photodiode shown in Fig. 1. The device architecture considered assumes abrupt interfaces and abrupt doping profiles (abrupt junction). The geometry consists of a 3.0 μm thick narrow-gap $Hg_{0.555}Cd_{0.445}Te$ absorber layer (AL), followed by a 1.0 μm thick wide-gap $Hg_{0.260}Cd_{0.740}Te$ cap layer (CL). The device has been engineered such that the AL bandgap wavelength is $\lambda = 2.575\,\mu$m and the 50% response cut-off wavelength is $\lambda_c = 2.521\,\mu$m at 200 K. Both the narrow-gap AL and the wide-gap CL are assumed to be identically doped n-type in the range $N_D = 1.0 \times 10^{15}-$

a)Electronic mail: jonathan.schuster2.ctr@mail.mil

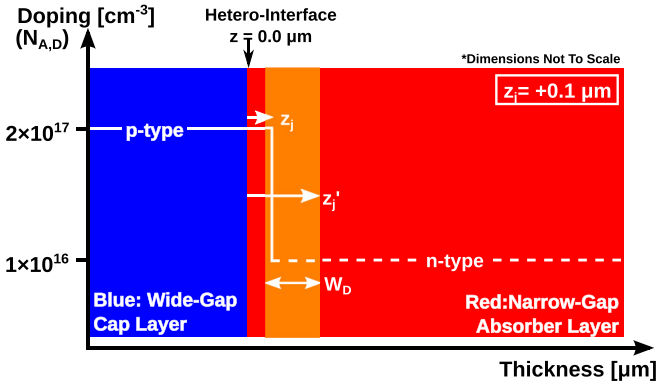

FIG. 1. Schematic representation of a single planar P^+-on-n HgCdTe pixel, where red and blue represent the narrow- and wide-gap layers, respectively, doping concentrations are given by the $y-$axis, $W_D(V)$ is the depletion region (light shaded region), z_j and $z_j'(V)$ are the implant depth and depletion region penetration, respectively (relative to the hetero-interface, based on the notation of Grimbergen[8]).

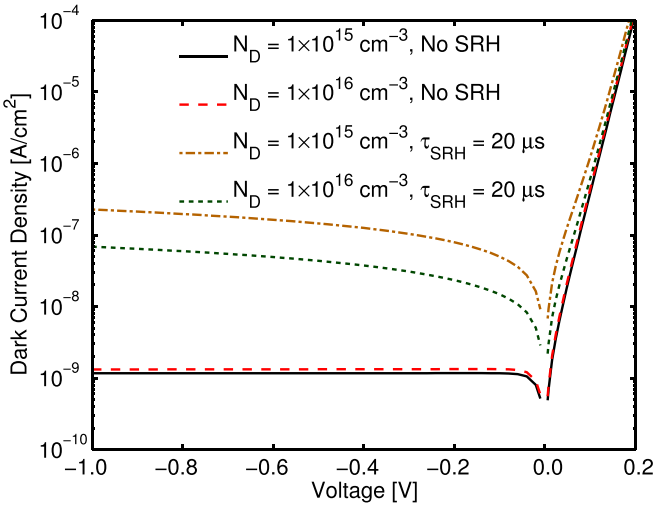

FIG. 2. Dark current versus voltage for $z_j = 0.0\,\mu$m.

$1.0 \times 10^{16}\,\text{cm}^{-3}$. In planar geometries, the junction is formed by implanting arsenic into the wide-gap CL, usually extending into the narrow-gap AL. In the numerical model, the p-type arsenic implant has been modeled as an abrupt profile with $N_A = 2.0 \times 10^{17}\,\text{cm}^{-3}$ (prior to doping compensation). The depth of the arsenic implant (measured from the AL/CL interface) is given by z_j. In the current analysis, the depth of the implant will be varied. A value of $z_j = 0\,\mu$m indicates that the implant terminates at the AL/CL interface, $z_j > 0\,\mu$m indicates that the implant extends into the narrow-gap AL (case shown in Fig. 1), and $z_j < 0\,\mu$m indicates that the implant resides solely in the CL. Dependent on z_j is also $z_j'(V)$, the extent to which the n-side depletion region ($W_{Dn}(V)$) penetrates into the AL (measured from the AL/CL interface), which is bias dependent, and must penetrate into the AL for collection of diffusion current and suitable device operation. A key parameter of this device is the valence band offset (ΔE_v) between the AL and CL. Calculating intrinsically ΔE_v using the electron affinities and energy gaps yields $\Delta E_v = 91$ meV which is significantly smaller than in other semiconductor systems used in SWIR detection, such as the $In_{0.53}Ga_{0.47}As$/InP heterostructure ($\Delta E_v = 440$ meV).[3] The model assumes ideal Ohmic contacts on the AL (fixed at zero bias) and CL (biased).

To simulate the device in Fig. 1, a two-dimensional (2D) finite element method implementation is used to solve Poisson's equation and the continuity equations.[9] The numerical model is discussed in detail in Ref. 10, where it has been used in three-dimensions (3D) to simulate pixel arrays. A 2D model has been used in the current analysis since the focus here is on studying effects along the growth direction and not lateral/3D effects. Additionally, band-to-band or trap-assisted tunneling currents, potentially prevalent in LWIR HgCdTe,[5] are not incorporated since they are not experimentally observed in SWIR HgCdTe due to the much larger bandgap and higher operating temperature.[11] A full description of the HgCdTe material parameters used is given in Ref. 12. In all simulations, unless otherwise specified, the device specifications are $N_D = 1.0 \times 10^{16}\,\text{cm}^{-3}$, $\Delta E_v = 91$ meV, $\tau_{SRH} = 20\,\mu$s, the temperature is $T = 200$ K, and when illumination is present $\lambda = 2.0\,\mu$m with an incident photon flux $\phi = 1 \times 10^{12}\,\text{photons cm}^{-2}\,\text{s}^{-1}$.

Figure 2 presents the dark J(V) characteristics of the detector shown in Fig. 1 with $z_j = 0.0\,\mu$m for two different absorber doping concentrations, with and without SRH recombination. Note that SRH recombination introduces current in two contributions: SRH recombination in the quasi-neutral region (diffusion current) and G-R in the depletion region.[13,14] To elucidate the numerical results in Fig. 2, consider analytically the diffusion reverse bias saturation current in the AL given by

$$J_{SAT} = qn_i^2 d\left(\frac{1}{\tau_{Tot} N_D}\right) = qn_i^2 d\left(B + C_n N_D + \frac{1}{\tau_{SRH} N_D}\right), \tag{1}$$

where J_{SAT} is the saturation current density (diffusion), q is the elemental charge, τ_{Tot} is the total lifetime, $d = t - W_{Dn}(V)$, t is the AL thickness, n_i is the intrinsic carrier concentration, B is the radiative capture probability, C_n is the Auger electron coefficient, and τ_{SRH} is the SRH lifetime for

TABLE I. AL properties due to Auger (calculated using $F_1F_2 = 0.10$), radiative (omitting photon recycling[15]), and SRH recombination. J_{SAT} calculated analytically using the values of $W_{Dn}(V = -0.100\,\text{V}) = 0.829\,\mu$m ($N_D = 10^{15}\,\text{cm}^{-3}$) and $0.263\,\mu$m ($N_D = 10^{16}\,\text{cm}^{-3}$).

N_D (cm^{-3})	B (cm^{-3}s^{-1})	C_n (cm^{-6}s^{-1})	τ_{Rad} (μs)	τ_{Aug} (μs)	τ_{SRH} (μs)	τ_{Tot} (μs)	$\tau_{Tot}N_D$ (cm^{-3}s)	J_{SAT} (A/cm^2)
1×10^{15}	6.51×10^{-11}	1.60×10^{-27}	15.35	625.15	N/A	14.99	1.50×10^{10}	8.01×10^{-10}
					20	8.57	8.57×10^{9}	1.40×10^{-9}
1×10^{16}	6.51×10^{-11}	1.60×10^{-27}	1.54	6.25	N/A	1.23	1.23×10^{10}	1.23×10^{-9}
					20	1.16	1.16×10^{10}	1.30×10^{-9}
					1	0.55	5.52×10^{9}	2.74×10^{-9}

electrons and holes. Recall Eq. (1) applies only to the quasi-neutral region and is a simplification (assuming low level injection and the thin base limit) of the continuity equations which are self-consistently solved in the numerical model. Utilizing the lifetime values given in Table I and the simulation results in Fig. 2, it is seen that the diffusion limited current saturates near $\approx 1\text{nA/cm}^2$. For $N_D = 1.0 \times 10^{15}\,\text{cm}^{-3}$, J_{SAT} is strictly due to radiative recombination and from Eq. (1) it is seen that when radiative recombination is dominant that J_{SAT} is independent of doping and depends linearly on B. However, when $N_D = 1.0 \times 10^{16}\,\text{cm}^{-3}$, Auger recombination contributes more significantly and J_{SAT} increases slightly but is still limited by radiative recombination. Observe that J_{SAT} remains nearly constant because the product $\tau_{\text{Tot}} N_D$ remains nearly constant as a function of doping when limited by radiative recombination. Note that incorporating photon recycling[15] would not alter these conclusions, although the transition from radiative to Auger dominated dark current would occur at lower doping concentrations. Introducing a modest $\tau_{\text{SRH}} = 20\,\mu\text{s}$ ($\tau_{n0} = \tau_{p0} = 20\,\mu\text{s}, E_{\text{trap}} = E_i$, Eq. (5.5) in Ref. 13) results in the dark current increasing by approximately two orders of magnitude (see Fig. 2), due to the very large contribution of G-R in the depletion region.[13,14] Since the SRH lifetime is longer than the radiative lifetime, the SRH contribution in the quasi-neutral region is minor (see Table I), however, the G-R depletion region current is over an order of magnitude higher and scales with the depletion region width and the intrinsic carrier concentration.[14] Consequently, since the higher doped device has a smaller depletion region ($W_{Dn} \sim 0.238\,\mu\text{m}$ ($N_D = 10^{16}\,\text{cm}^{-3}$) compared to $W_{Dn} \sim 0.744\,\mu\text{m}$ ($N_D = 10^{15}\,\text{cm}^{-3}$) at zero bias, calculated analytically using $x = 0.445$), the dark current is lower with the higher doping (see Fig. 2). Therefore, increasing the doping reduces the dark current since a higher doping shrinks the depletion region, reducing the G-R current.

In Fig. 2, it was shown that when SRH recombination is present that the dominant contribution to the dark current is from G-R in the depletion region and that increasing the doping decreases the depletion region width thereby reducing the dark current. Therefore, to reduce the G-R dark current further, the depletion region must be reduced in size by increasing the doping or the depletion region must be shifted into the wide-gap CL.[4] Adopting the second option, the depletion region can be shifted into the CL by reducing the implant depth (z_j), such that the implant resides solely in the CL ($z_j < 0\,\mu\text{m}$ in Fig. 1). However, great care must be placed in choosing the implant depth when utilizing this optimization technique. This design choice can result in a bias dependent QE if the depletion region ($z_j'(V)$ in Fig. 1) does not penetrate slightly into the AL near zero bias.[4] Given that $z_j'(V) \sim \sqrt{|V|}$, reverse bias must then be applied to extend $z_j'(V)$ into the AL to collect photocurrent. Towards this end, Fig. 3 presents the dark J(V) characteristics (a) and internal QE (b) for several values of z_j, QE calculated using Eq. (16) in Ref. 10. When the junction extends into the AL ($z_j = +0.1\,\mu\text{m}$) or terminates at the AL/CL interface ($z_j = 0.0\,\mu\text{m}$), the dark current and QE are identical for each case as a function of voltage. In both cases, the dark current is due to G-R at all biases and the QE is voltage independent. However, as the junction is shifted sufficiently into the wide-gap CL ($z_j \leq -0.2\,\mu\text{m}$), the dark current at small to moderate reverse bias initially saturates as a diffusion current before G-R contributes at larger reverse bias. As the reverse bias is further increased, the depletion region expands further into the AL and the G-R current approaches that of the $z_j \geq 0\,\mu\text{m}$ cases. However, to adequately observe the initial G-R suppression, the junction must reside sufficiently in the wide-gap CL, which is why diffusion limited behavior is not observed when $z_j = -0.1\,\mu\text{m}$ (although the dark current in magnitude is noticeably lower).

Figure 4 presents the dark current (a) and QE (b) versus z_j at a fixed bias of $V = -0.100$ V with and without SRH recombination. Consider first the case without SRH recombination. The dark current is equal to J_{SAT} when the junction is located in the AL ($z_j = +0.1\,\mu\text{m}$). As the junction is shifted into the CL, the dark current remains at J_{SAT} until is begins to progressively decrease near $z_j \sim -0.25\,\mu\text{m}$. At $z_j = -0.25\,\mu\text{m}$, $z_j'(V)$ does not penetrate sufficiently into the AL (at this bias), which prevents the collection of thermally (and optically) generated carriers via diffusion. Consequently, the same suppression is seen in the QE, since the diffusion dark current and photocurrent are both mutually dependent diffusion processes. However, even at $z_j \sim -0.25\,\mu\text{m}$, QE $\approx 90\,\%$. Consider, now $\tau_{\text{SRH}} = 20\,\mu\text{s}$. For

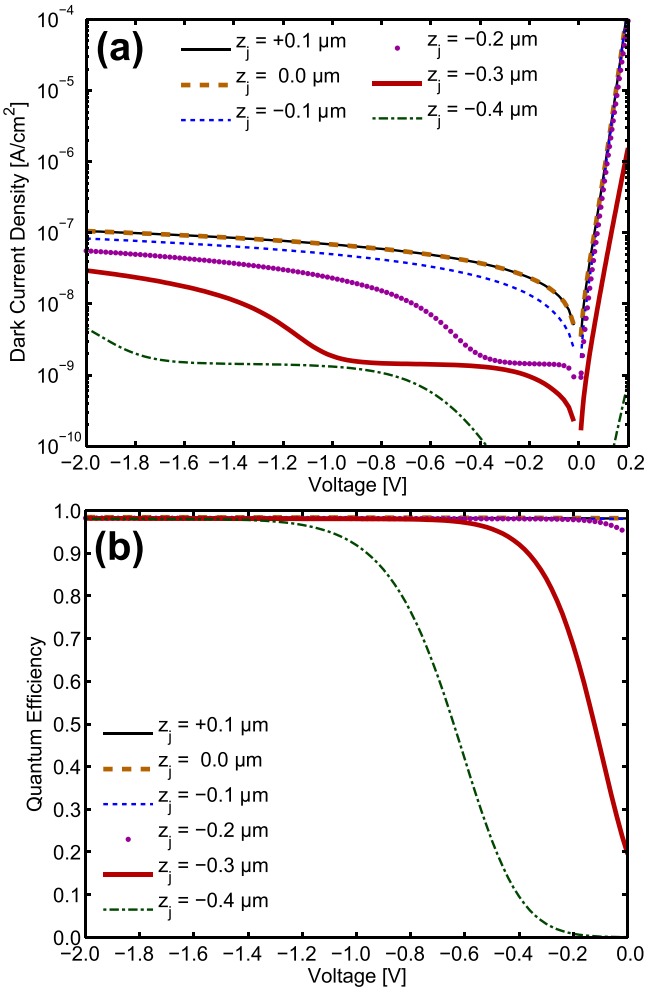

FIG. 3. Dark current (a) and internal QE (b) versus voltage for several values of z_j.

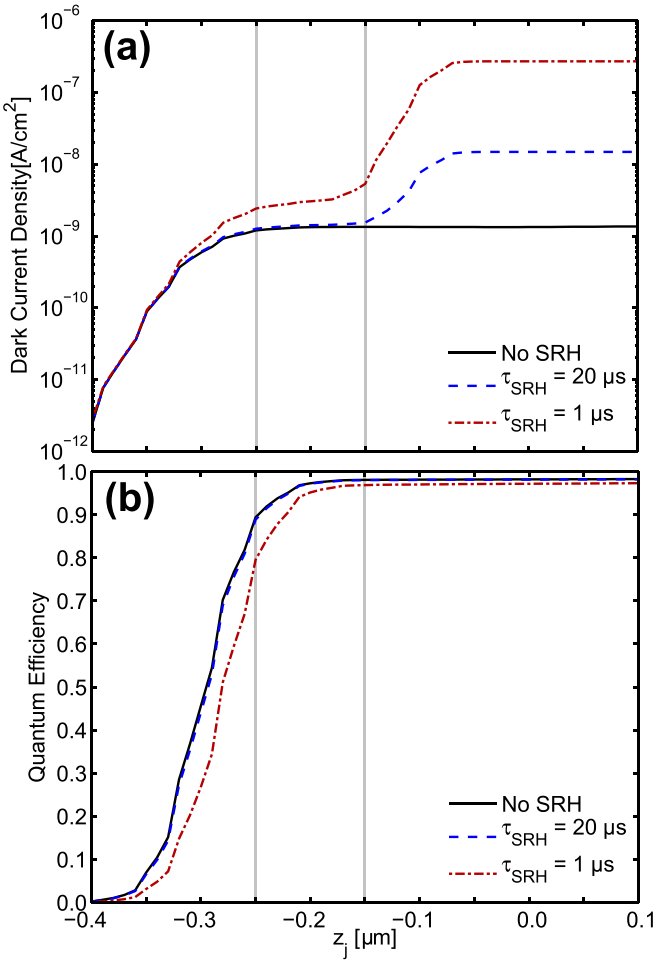

FIG. 4. Dark current (a) and internal QE (b) versus z_j at -0.100 V.

$z_j > -0.15\,\mu$m, G-R now contributes significantly to the dark current since the majority of $z_j'(V)$ resides in the narrow-gap AL. However, as $z_j \to -0.15\,\mu$m, $z_j'(V)$ resides progressively in the wide-gap CL, eliminating the G-R current. Most importantly, the G-R current turns off before the diffusion current does. Thus there is an optimal regime where the dark current is diffusion limited, without significantly reducing the QE, despite $\tau_{SRH} = 20\,\mu$s. This optimum resides within $-0.25\,\mu\text{m} \lesssim z_j \lesssim -0.15\,\mu$m (depicted by grey lines in Fig. 4). The same benefits are observed for the worst case scenario of $\tau_{SRH} = 1\,\mu$s. The dark current reduction is seen, although the diffusion current is larger since SRH recombination now contributes in the quasi-neutral region as well ($\tau_{SRH} < \tau_{Rad}$, see Table I).

Given that the results presented in Fig. 4 are bias dependent, it is desirable to devise a figure of merit to optimize z_j that is independent of reverse bias. This can be achieved by utilizing solar cells metrics and calculating under forward bias the fill factor[16] $FF = (I_{MP}V_{MP})/(I_{sc}V_{oc})$, where I_{MP} and V_{MP} are the current and voltage that correspond to where $P = IV$ is maximum, V_{oc} is the open circuit voltage, and I_{sc} is the short circuit current, given by $-I_{sc} = I_{\text{Photo}}|_{V=0.0\,\text{V}}$ and $V_{oc} = V(I_{\text{Dark}} = I_{\text{Photo}})$. Note that I_{sc} and V_{oc} depend on both the dark current and incident photon flux. Figure 5 presents the fill factor versus z_j. It is observed that when SRH recombination is prevalent that FF initially increases as z_j is

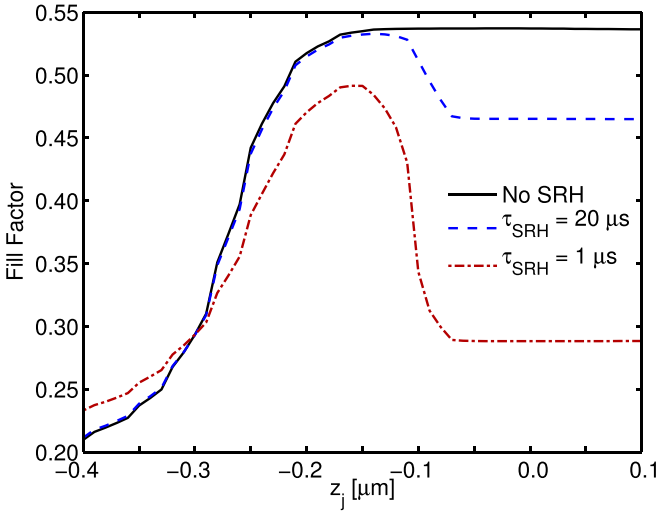

FIG. 5. Fill factor versus z_j.

decreased and reaches a maximum at the value of z_j where diffusion limited behavior is observed (compare to Fig. 4(a)). After this peak, FF continually decreases as $z_j \to -0.40\,\mu$m to a minimum value far below the initial value at $z_j = +0.1\,\mu$m. Therefore, calculating FF yields a metric, independent of reverse bias, that provides the largest value of z_j with diffusion limited performance (corresponding to where FF is maximized).

In conclusion, heterojunction device design concepts have been leveraged to suppress G-R dark current in SRH limited eSWIR HgCdTe P^+-on-n infrared detectors by shifting the arsenic implant into the wide-gap CL. Numerical simulations were performed to study the dependence of the device performance on implant depth, layer doping, lifetime (specifically SRH), and detector bias. The simulations reveal that by properly designing the depletion region, the implant can be confined to the wide-gap layer without reducing the QE, thereby significantly reducing G-R attributed dark current. This technique is possible in HgCdTe due to the relatively small ΔE_v but may not be optimal in material systems with significantly larger ΔE_v. Finally, these design rules should only be leveraged in G-R limited material and will not yield superior device performance in diffusion limited material.

This work was supported in part by an appointment to the U.S. Army Research Laboratory Postdoctoral Fellowship Program administered by the Oak Ridge Associated Universities (ORAU) through a contract with the U.S. Army Research Laboratory.

[1]Y. Arslan, F. Oguz, and C. Besikci, Infrared Phys. Technol. **70**, 134 (2015).
[2]R. T. Littleton, J. S. C. Acad. Sci. **6**, 24 (2008).
[3]A. R. Wichman, R. E. DeWames, and E. Bellotti, Proc. SPIE **9070**, 907003 (2014).
[4]W. E. Tennant, E. C. Piquette, D. L. Lee, M. L. Thomas, and M. Zandian, U.S. patent 7,368,762 B2 (6 May 2008).
[5]M. B. Reine, Proc. SPIE **4288**, 266–277 (2001).
[6]E. A. Kraut, J. Vac. Sci. Technol. A **7**, 420 (1989).
[7]R. DeWames, R. Littleton, C. Billman, J. Pellegrino, S. Horn, and R. Balcerak, The US Workshop on the Physics and Chemistry of II-VI Materials, Las Vegas, NV, 2008.

[8]C. A. Grimbergen, Solid-State Electron. **19**, 1033 (1976).
[9]Synopsys, "Sentaurus device user guide," 2013, version H-2013.03.
[10]J. Schuster, B. Pinkie, S. Tobin, C. Keasler, D. D'Orsogna, and E. Bellotti, IEEE J. Sel. Top. Quantum Electron. **19**, 3800415 (2013).
[11]S. Simingalam, B. VanMil, Y. Chen, E. DeCuir, Jr., G. Meissner, P. Wijewarnasuriya, N. Dhar, and M. Rao, Solid-State Electron. **101**, 90 (2014).
[12]D. D'Orsogna, Ph.D. dissertation, Boston University, Boston, MA, 2010.
[13]W. Shockley and W. T. Read, Jr., Phys. Rev. **87**, 835 (1952).
[14]S. C. Choo, Solid-State Electron. **11**, 1069 (1968).
[15]R. G. Humphreys, Infrared Phys. **23**, 171 (1983).
[16]H. J. Hovel, "Solar cells," *Semiconductors and Semimetals* (Academic, 1975), Vol. 11, pp. 5, 37–63.